Scripta Materialia 178 (2020) 193–197

Contents lists available at ScienceDirect

Scripta Materialia

journal homepage: www.elsevier.com/locate/scriptamat

Atomic segregation at twin boundaries in a Mg-Ag alloy

X.F. Chen[a,b], L.R. Xiao[c], Z.G. Ding[c,*], W. Liu[c], Y.T. Zhu[c,d], X.L. Wu[a,b,**]

[a] State Key Laboratory of Nonlinear Mechanics, Institute of Mechanics, Chinese Academy of Sciences, Beijing 100190, China
[b] School of Engineering Sciences, University of Chinese Academy of Sciences, Beijing 100049, China
[c] Nano and Heterogeneous Materials Center, School of Materials Science and Engineering, Nanjing University of Science and Technology, Nanjing 210094, China
[d] Department of Materials Science & Engineering, North Carolina State University, Raleigh, NC 27695, USA

ARTICLE INFO

Article history:
Received 20 August 2019
Revised 17 October 2019
Accepted 9 November 2019
Available online 21 November 2019

Keywords:
Segregation
Twin boundary
Magnesium alloy
HAADF-STEM

ABSTRACT

Segregation of solute atoms at twin boundaries (TBs) plays a critical role in mechanical properties and thermal stability of magnesium alloys. Here, segregation structures at $\{10\bar{1}1\}$, $\{10\bar{1}2\}$ and $\{10\bar{1}3\}$ TBs are characterized in a Mg-Ag alloy by means of the atomic resolution high-angle annular dark-field technique based on scanning transmission electron microscopy. Of particular finding is the unique complex segregation at $\{10\bar{1}3\}$ TBs, where Ag atoms occupy both substitutional and interstitial sites. By contrast, Ag atoms only substitutionally segregate at $\{10\bar{1}1\}$ and $\{10\bar{1}2\}$ TBs. Calculation simulation of segregation energy and three-dimensional structure of TBs helps understanding of hybrid segregation.

Recently, considerable concerns have arisen on the segregation of solute atoms at twin boundaries (TBs) in magnesium alloys [1–4], which may potentially lead to an enhancement of both strength and thermal stability etc. [5,6]. The pioneer work by Nie et al. [1] reported a periodic segregation of both Gd and Zn atoms along $\{10\bar{1}1\}$, $\{10\bar{1}2\}$ and $\{10\bar{1}3\}$ TBs in binary Mg-Gd and ternary Mg-Gd-Zn alloys. The segregation sites depend on the radius of solute atoms, relative to that of magnesium [1,7]. Larger and smaller ones go to tension and compression sites near TBs, respectively. Further, the lattice structure of atomic segregation varies. A complex spinal-shaped segregation was observed near $\{10\bar{1}2\}$ TBs in a quinary Mg-Gd-Y-Ag-Zr alloy [8,9]. Up to date, only substitutional segregation was observed [10]. This is, on the surface, in line with substitutional-type precipitates of varying kinds. This is due to the replacement of magnesium atoms with those of relatively large radius in terms of the Hume-Rothery rule [11].

Yet, two issues are still unclear concerning atomic segregation at TBs in magnesium alloys. First, besides atomic radius, whether or not atomic segregation is still affected by other facts, such as structures of twin boundary. Second, whether or not only the substitutional-type segregation exists. Its importance lies in that the interstitial-type segregation probably serves as an incentive of interstitial-type precipitate. This contributes to strengthening and thermal stability more effectively than substitutional precipitates. Here, a simple binary Mg-2.57Ag (weight%) alloy was selected as a model alloy to answer aforesaid two questions.

The starting Mg-Ag ingot had a dimension of $20 \times 30 \times 6$ mm^3. The fabrication method was detailed in [12]. The ingot was hot rolled at 500 °C with thickness reduction of 35%, followed by annealing at 300 °C for 30 min to obtain a fully recrystallized microstructure. Then, cold rolling with 20% of thickness reduction was performed, followed by annealing at 150 °C for 30 min to facilitate atomic segregation.

Cross-sectional TEM specimens were cut from rolled sheet and gently polished to a thickness of ~60 μm, followed by a precise dimple grinding to ~25 μm thick. Perforation was performed by low angle (<3.5°) and low energy (<3 KeV) ion milling on a cold stage (−30 °C). The atomic-resolution high-angle annular dark field (HAADF) observations were carried out on an aberration-corrected scanning transmission electron microscope (STEM) (FEI Titan G^2 60–300) operated at 300 kV. The collection angle, central collection half angle and camera length were set as 15 mrad, 76 mrad and 100 nm, respectively.

The density functional theory (DFT) calculations were carried out using the Vienna Ab Initio Simulation Package [13]. The interaction between the valence electrons and ionic cores was described by the projector augmented wave (PAW) method [14]. The generalized gradient approximation (GGA) with the Perdew–Burke–Ernzerhof (PBE) approximations was used as the exchange-correlation functional [15,16]. The cut-off energy was set as 400 eV.

* Corresponding author.
** Corresponding author at: State Key Laboratory of Nonlinear Mechanics, Institute of Mechanics, Chinese Academy of Sciences, Beijing 100190, China.
E-mail addresses: zhigangding@njust.edu.cn (Z.G. Ding), xlwu@imech.ac.cn (X.L. Wu).

https://doi.org/10.1016/j.scriptamat.2019.11.025
1359-6462/

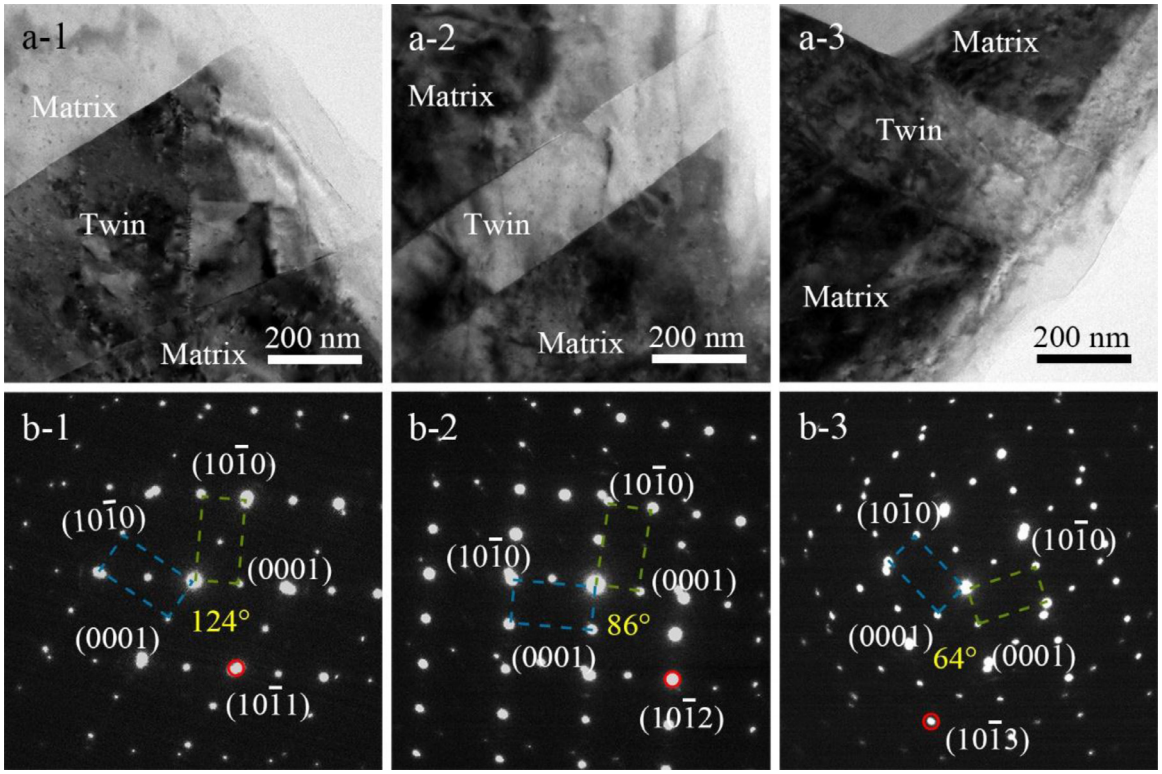

Fig 1. TEM images in Mg-Ag alloy. (a-1) to (a-3) {10$\bar{1}$1}, {10$\bar{1}$2}, and {10$\bar{1}$3} twin plates; (b-1) to (b-3) Corresponding SAED patterns.

A Monkhorst-Pack k-point mesh of 18 × 18 × 12 was used for the Mg and Ag hexagonal unit cell. The same k-point mesh density was applied to other super-cells. With the selected cut-off energy value and the k-point mesh, the calculated values of total energy converged to within 1 meV/atom. The atomic structures were fully relaxed using a conjugate gradient algorithm. The atomic structures were judged to have fully relaxed when the force acting on each atom was smaller than 0.010 eV/Å.

Deformation twinning systems of three kinds exist usually in Mg alloys, including {10$\bar{1}$1}, {10$\bar{1}$2}, and {10$\bar{1}$3} [17,18]. The {10$\bar{1}$2} twin is extension type to produce elongation along the c-axis, while the remaining two are compression twins [19]. Fig. 1a-1–a-3 is three TEM bright-field images showing, respectively, {10$\bar{1}$1}, {10$\bar{1}$2}, and {10$\bar{1}$3} twin plates in the present Mg-Ag alloy. The corresponding selected area electron diffraction (SAED) patterns are shown in Fig. 1b-1–b-3. The basal plane (0001) is parallel to the observation direction. It can be observed that the angle between the $\{0001\}_\alpha$ plane for the matrix and $\{0001\}_\alpha$ plane for twin plates is, respectively, 124°, 86° and 64°.

The exact atomic position and lattice structure can be accurately determined by the atomic-resolution image of aberration-corrected TEM due to a ultra-high spatial resolution to as large as ~0.8 Å. Moreover, the chemical composition of each atomic column can be distinguished by the Z constrast in HAADF-STEM images. Consequently, the brighter atomic columns represent the Ag-rich columns in Mg-Ag alloy in this work. Fig. 2a-1 and b-1 is HAADF-STEM images of low magnification, showing {10$\bar{1}$1} and {10$\bar{1}$2} TBs, respectively, along [1$\bar{2}$10] zone axis. Both TBs appear zigzag, consisting of incoherent steps of several atomic-layer thick. The twin dislocations distributed along the incoherent TBs are proposed to tilt the TBs slightly in [20]. The segregation of Ag atoms is visible along both TBs. The corresponding fast Fourier transform (FFT) patterns, as shown in Fig. 2a-2 and b-2, correspond with the experimental diffraction patterns (Fig. 1b-1 and b-2). Fig. 2a-3 and b-3 is the atomic-resolution HAADF-STEM images. Segregation along a single row is observed in {10$\bar{1}$1} and {10$\bar{1}$2} TBs, similar to the TB segregation as reported in both Mg-Gd and Mg-Zn alloy [1]. The atoms at TBs of Mg alloys are not perfectly close-packed. As a result, the compression site and tension site alternate [1]. The space of the former is smaller than that a Mg atom would occupy, whereas the tension site is larger. For this reason, the solute atoms larger than Mg tend to segregate to tension sites, while smaller ones go to the compression sites. Therefore, the atoms of Ag will replace Mg atoms in compression sites due to the smaller radius of Ag (0.144 nm) than that of Mg (0.160 nm). From the atomic structure models (Fig. 2a-4 and b-4), purple and yellow spheres represent atoms in layers A and B in magnesium matrix, respectively. Red spheres represent Ag atoms that have brighter contrast in HAADF-STEM images (Fig. 2a-1/a-3 and 2b-1/b-3). Hence, Ag atoms segregate substitutionally at the compression sites in both {10$\bar{1}$1} and {10$\bar{1}$2} TBs.

Fig. 3a is the HAADF-STEM image of low magnification, revealing zigzag segregation along a {10$\bar{1}$3} TB as evidenced by the FFT diffraction pattern (Fig. 3b). Interestingly, a unique segregation structure appears in the atomic-resolution HAADF-STEM image (Fig. 3c). Specifically, the periodic segregation unit, with three Ag-rich columns in each unit, forms along the {10$\bar{1}$3} TB. This structure is indicative of a complex type of interstitial and substitutional segregation. The segregation is different from single substitutional one at both {10$\bar{1}$1} and {10$\bar{1}$2} TBs and has never been reported before.

The model of atomic structure is proposed and further marked on the atomic-resolution image as shown in Fig. 3d to distinguish different Z-contrasts caused by varying elements. In terms of Eq. (1) [21], the intensity of atomic columns in a HAADF image is approximately proportional to the square of the atomic number Z, i.e.,

$$\sigma_{(\theta)} = \frac{e^4 Z^2 d\Omega}{16(4\pi\varepsilon_0 E_0)^2 \sin^4 \frac{\theta}{2}} \quad (1)$$

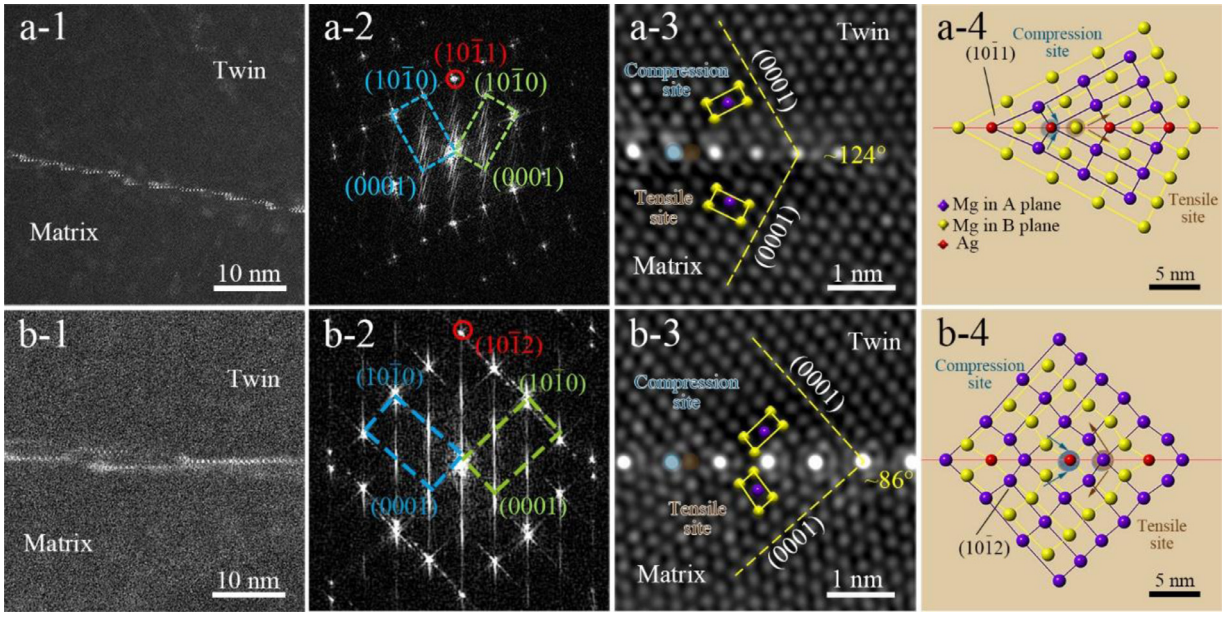

Fig 2. Substitutional segregation of Ag atoms at {10$\bar{1}$1} (a-) and {10$\bar{1}$2} (b-) twin boundaries, respectively. (a-1/b-1) HAADF-STEM images of low magnification in zone axis of [1$\bar{2}$10]; (a-2/b-2) FFT patterns; (a-3/b-3) HAADF-STEM images of high magnification; (a-4/b-4) Atomic structural models. (For interpretation of the references to color in this figure, the reader is referred to the web version of this article.)

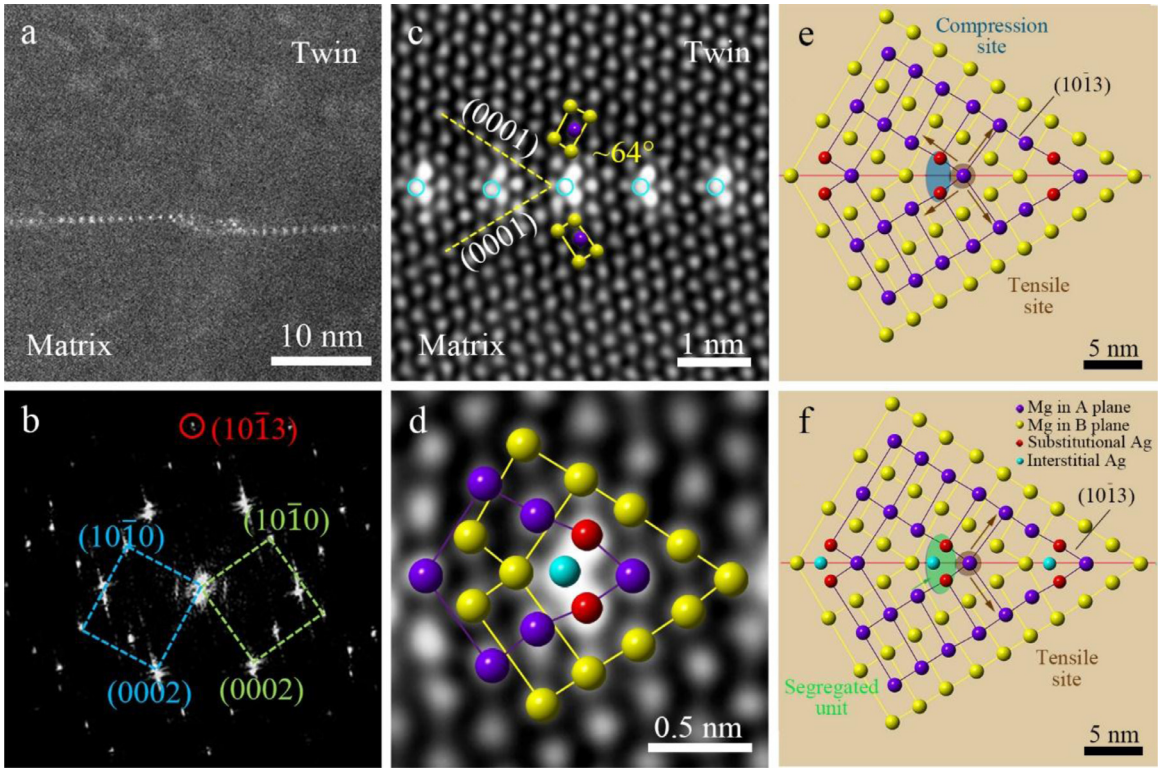

Fig 3. Complex segregation at {10$\bar{1}$3} twin boundary. (a) HAADF-STEM image of low magnification in zone axis of [1$\bar{2}$10]; (b) FFT pattern; (c) Atomic resolution HAADF-STEM image; (d) Close-up of (c); (e) and (f) Two-dimensional models of substitutional and interstitial segregation at {10$\bar{1}$3} twin. (For interpretation of the references to color in this figure, the reader is referred to the web version of this article.)

where σ is scattering cross section, θ is scattering semi-angle, Ω is solid angle, e is electron charge, Z is atomic number, ε_0 is the dielectric constant and E_0 is energy of the electrons.

From the atomic structure model as shown in Fig. 3e and f, the purple and yellow spheres represent atoms in layers A and B in magnesium matrix, respectively. The red and turquoise spheres represent the substitutional and interstitial segregations of Ag atoms, respectively. The interfacial segregation in {10$\bar{1}$3} twin of Mg-Ag alloy can be separated into two non-sequential parts. One is the substitutional segregation as shown in Fig. 3e, in which Mg atoms in compression sites are replaced by Ag atoms, as marked by red atoms. Another is the interstitial segregation as shown in Fig. 3f. An additional Ag atomic column is inserted in the position marked by turquoise spheres. Thus, a complex segregation is

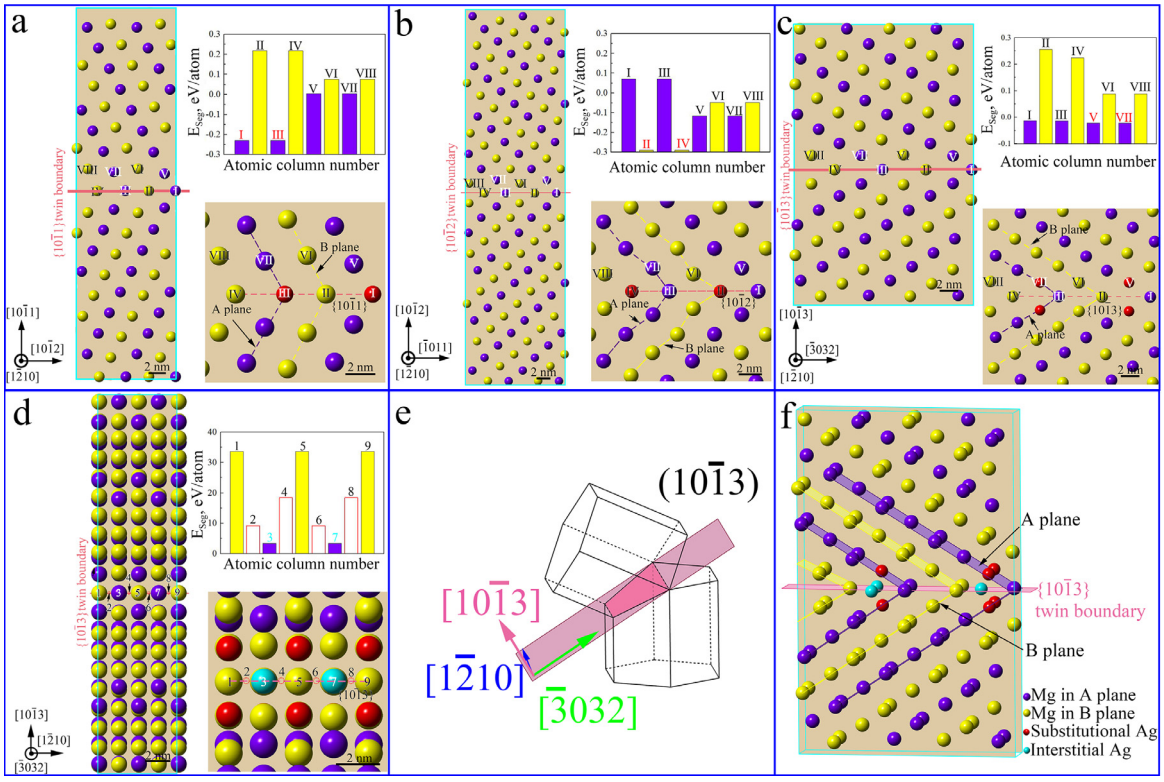

Fig 4. DFT calculations of segregation. (a) {10$\bar{1}$1} twin, (b) {10$\bar{1}$2} twin, (c) {10$\bar{1}$3} twin all in [1$\bar{2}$10] zone axis; (d) {10$\bar{1}$3} twin in [$\bar{3}$032] zone axis; (e) Diagram of [1$\bar{2}$10] and [$\bar{3}$032] zone axes with (10$\bar{1}$3) twin; (f) Three-dimensional structure of hybrid Ag in {10$\bar{1}$3} twin. Purple and yellow spheres represent atoms in layers A and B of the Mg lattice, respectively; red and turquoise spheres represent substitutional and interstitial segregations of Ag atoms, respectively; pink planes represent the twin boundaries of Mg. (For interpretation of the references to color in this figure legend, the reader is referred to the web version of this article.)

formed in {10$\bar{1}$3} twin, which is composed by interstitial and substitutional segregations.

TEM images provide a two-dimensional projection lattice structure instead of atomic positions in the direction perpendicular to the screen. In case of substitutional segregation, the spatial position of atoms was usually analyzed with assistance of the lattice of Mg matrix, because each solute atom replaced a Mg atom, and occupied its position in interface [22,23]. Concerning composite segregation, however, it is impossible to locate interstitially segregated atoms in the lattice. Thus, first principle calculation was performed to assist the reconstruction of three-dimensional structure of TB segregation.

Super-cells of twins were built in DFT calculations, where TBs were represented by pink lines, as shown in Fig. 4a–d. The procedure of super-cell construction can be found in [24]. The segregation energy (E_{seg}) was defined as the reduction in the total system energy when a solute atom segregates to TB, which was calculated by Eq. (2),

$$E_{seg} = \{[E_{Twin}(Mg_{N-m}X_m) - E_{Twin}(Mg_N)] - m[E_{Matrix}(Mg_{M-1}X) - E_{Matrix}(Mg_M)]\}/m \quad (2)$$

where $E_{Twin}(Mg_{N\text{-}m}X_m)$ is the total energy of a supercell containing TB. N is the number of atoms in super-cell, N-*m* is the number of Mg atoms and m is the number of solute atoms X(Ag) in segregated atoms. $E_{Twin}(Mg_N)$ is the total energy of a pure Mg super-cell containing TBs. $E_{Matrix}(Mg_{M\text{-}1}X)$ is the total energy of a TB-free supercell with (M-1)Mg atoms and 1 Ag atom. $E_{Matrix}(Mg_M)$ is the total energy of a pure and perfect Mg super-cell with M Mg atoms. The TB segregation energy was normalized by the number of segregated atoms *m*. The solute segregation was then analyzed based on calculated E_{seg}. The Ag atoms prefer to segregate at the columns with negative E_{seg}. The lowest E_{seg} represents the most preferred position for segregation. Fig. 4a and b shows the DFT calculation of E_{seg} in {10$\bar{1}$1} and {10$\bar{1}$2} twins of Mg-Ag alloy, respectively. Substitutional segregations of Ag in columns numbered by I to VIII were calculated individually. The DFT calculation reveals that the compression sites of both twins had the lowest E_{seg}, i.e., Columns I and III in {10$\bar{1}$1} twin and Columns II and IV in {10$\bar{1}$2} twin, which is coincide with the experimental result as shown in Fig. 2.

The segregation in {10$\bar{1}$3} twins is a mixture of interstitial and substitutional one. On one hand, the substitutional segregation follows the same rule in {10$\bar{1}$1} and {10$\bar{1}$2} twins, as shown in Fig. 4c. Ag atoms segregated in Columns V and VII (compression sites), which have the lowest E_{seg} among all calculated columns. The lowest E_{seg} which is original from charge transferring (Fig. S1). Higher charge transfer from Mg to Ag indicated that Ag segregation was benefit for reducing twin boundary energy and stabilizing the twins.

On the other hand, the interstitial-type segregation was analyzed by combining both experimental and simulation results. Based on experimental observations (Fig. 3d), firstly, the location of interstitial Ag columns in the projection structure was determined. Secondly, the spatial positions of Ag atoms in the column (the [$\bar{3}$032] zone axis) were determined according to DFT calculation, where E_{seg} of nine positions (Points 1–9) were comparatively studied, as shown in Fig. 4d. The [$\bar{3}$032] zone axis is parallel to the (10$\bar{1}$3) plane, which is perpendicular to the [1$\bar{2}$10] zone axis, as illustrated in Fig. 4e. As shown in Fig. 4d, Points 3 and 7, locating in the middle of substitutional Ag atoms, have the lowest E_{seg}. Therefore, the substitutional and interstitial Ag columns in TEM images, namely red and turquoise spheres in Fig. 3d, are not in a same (11$\bar{2}$0) plane. The real three-dimensional structure of the hybrid Ag segregation was then established, as shown in Fig. 4f.

In summary, the segregation structures are investigated at $\{10\bar{1}1\}$, $\{10\bar{1}2\}$ and $\{10\bar{1}3\}$ twin boundaries using HAADF-STEM technique in a Mg-Ag binary alloy. The substitutional segregation of Ag appears in $\{10\bar{1}1\}$ and $\{10\bar{1}2\}$ twin boundaries. A distinct complex segregation is found at the $\{10\bar{1}3\}$ twin boundary, with two substitutional columns and one interstitial column in each periodic segregation unit. Computational simulations based on DFT reveals that Ag segregation occurs in the columns with lowest E_{seg}. In addition, the interstitial segregation was analyzed combining the both the experimental and simulated results. The model is established of a real three-dimensional structure to reveal the complex Ag segregation at $\{10\bar{1}3\}$ twin boundary.

Declaration of Competing Interest

The authors declare that they have no known competing financial interests or personal relationships that could have appeared to influence the work reported in this paper.

Acknowledgment

This work is supported by the National Key Research and Development Program of China (2017YFA0204402), the National Natural Science Foundation of China (grant numbers 51601003, 11672323, 11572328, 51901103 and 51601204), the Fundamental Research Funds for the Central Universities (grant number 30918011342), the U.S. Army Research Office (W911 NF-17-1-0350). The authors are thankful for the technical support from the Jiangsu Key Laboratory of Advanced Micro&Nano Materials and Technology, and the Materials Characterization Facility of Nanjing University of Science and Technology.

Supplementary materials

Supplementary material associated with this article can be found, in the online version, at doi:10.1016/j.scriptamat.2019.11.025.

References

[1] J.F. Nie, Y.M. Zhu, J.Z. Liu, X.Y. Fang, Science 340 (2013) 957–960.
[2] D.A. Basha, R. Sahara, H. Somekawa, J.M. Rosalie, A. Singh, K. Tsuchiya, Scr. Mater. 124 (2016) 169–173.
[3] M. Bugnet, A. Kula, M. Niewczas, G.A. Botton, Acta Mater. 79 (2014) 66–73.
[4] Y.M. Zhu, S.W. Xu, J.F. Nie, Acta Mater. 143 (2018) 1–12.
[5] H. Somekawa, H. Watanabe, D.A. Basha, A. Singh, T. Inoue, Scr. Mater. 129 (2017) 35–38.
[6] K. Leitner, D. Lutz, W. Knabl, M. Eidenberger-Schober, K. Huber, A. Lorich, H. Clemens, V. Maier-Kiener, Scr. Mater. 156 (2018) 60–63.
[7] X.Y. Shi, Y. Liu, J. Lu, R.E.A. Williams, D.J. Li, X.Q. Zeng, A.A. Luo, Scr. Mater. 112 (2016) 136–139.
[8] H. Zhou, G.M. Cheng, X.L. Ma, W.Z. Xu, S.N. Mathaudhu, Q.D. Wang, Y.T. Zhu, Acta Mater. 95 (2015) 20–29.
[9] L.R. Xiao, Y. Cao, S. Li, H. Zhou, X.L. Ma, L. Mao, X.C. Sha, Q.D. Wang, Y.T. Zhu, X.D. Han, Acta Mater. 162 (2019) 214–225.
[10] X.C. Sha, L.R. Xiao, X.F. Chen, G.M. Cheng, Y.D. Yu, D.D. Yin, H. Zhou, Philos. Mag. 99 (2019) 1957–1969.
[11] W. Hume-Rothery, W. Mabbott Gilbert, K.M. Channel Evans, Philos. Trans. 233 (1934) 1–97 the Royal Society of London A.
[12] H. Zhou, Q.D. Wang, J. Chen, B. Ye, W. Guo, Trans. Nonferrous Metals Soc. 22 (2012) 1891–1895.
[13] G. Kresse, J. Furthmüller, Comput. Mater. Sci. 6 (1996) 15–50.
[14] P.E. Blochl, Phys. Rev. 50 (1994) 17953–17979.
[15] J.P. Perdew, K. Burke, M. Emzerhof, Phys. Rev. Lett. 77 (1996) 3865–3868.
[16] G. Kresse, D. Joubert, Phys. Rev. 59 (1999) 1758–1775.
[17] J.W. Christian, S. Mahajan, Prog. Mater. Sci 39 (1995) 1–157.
[18] Y.T. Zhu, X.Z. Liao, X.L. Wu, Prog. Mater. Sci. 57 (2012) 1–62.
[19] H.H. Yu, C.Z. Li, Y.C. Xin, A. Chapuis, X.X. Huang, Q. Liu, Acta Mater. 128 (2017) 313–326.
[20] Y. Liu, X.F. Chen, K. Wei, L.R. Xiao, B. Chen, H.B. Long, Y.D. Yu, Z.H. Hu, H. Zhou, Materials 12 (2019) 1307–1314.
[21] D.B. Williams, C.B. Carter, Transmission electron microscopy: a textbook for materials Science, second ed., Springer, New York, 2009, p. 775.
[22] H. Zhou, W.Z. Xu, W.W. Jian, G.M. Cheng, X.L. Ma, W. Guo, S.N. Mathaudhu, Q.D. Wang, Y.T. Zhu, Philos. Mag. 94 (2014) 2403–2409.
[23] J. Zhang, Y.C. Dou, Y. Zheng, Scr. Mater. 80 (2014) 17–20.
[24] J.R. Morris, Y.Y. Ye, M.H. Yoo, Philos. Mag. 85 (2005) 233–238.